ELSEVIER

Journal of Power Sources 55 (1995) 217–230

JOURNAL OF POWER SOURCES

Mathematical modelling of a lead/acid cell with immobilized electrolyte

Johan Landfors [a], Daniel Simonsson [a], Artjom Sokirko [b,1]

[a] *Department of Chemical Engineering and Technology, Division of Applied Electrochemistry, The Royal Institute of Technology,* **10044** *Stockholm, Sweden*

[b] *Department of Mechanics, Division of Hydromechanics, The Royal Institute of Technology,* **10044** *Stockholm, Sweden*

Received **24** September **1994;** in revised form 7 February **1995;** accepted 8 February 1995

Abstract

A mathematical model has been developed for a lead/acid cell with immobilized electrolyte, using the transport equations for concentrated electrolyte solutions and experimentally determined kinetic equations for the two porous electrodes. The model equations have been solved by means of an algorithm, which gives, after discretization of the differential equations, a single tridiagonal coefficient matrix for the concentration profile over the whole multi-region system consisting of a positive electrode, a separator and a negative electrode, respectively. The model can be used for optimization of the actual type of lead/acid cell for different applications. The numerically predicted results are in fair agreement with experimental data for acid and lead sulfate concentration profiles in a cell, although the experimentally measured acid concentration in the negative electrode after discharge is generally lower than the calculated value, and the predicted discharge time is lower than the experimental ones at high discharge rates.

Keywords: Lead/acid cells; Sulfuric acid; Immobilized electrolytes

1. Introduction

Mathematical modelling of the lead/acid battery is a powerful tool in the attempt to analyse, predict and optimise its performance, both in its traditional applications as a car battery for starting, lighting and ignition or as a truck battery, as well as in new applications such as uninterrupted power supply, load levelling and electric cars. Mathematical models for the lead/acid cell have been reported earlier. A porous electrode model for the positive plate was extended first to the negative plate and then to the complete cell by Micka and Roušar [1]. They assumed that the electrolyte between the two plates is well mixed by free convection and they calculated its mean concentration from an integral material balance for the sulfuric acid. The discharge process was simulated and the discharge time was calculated as a function of the plate distance. The discharge time was taken to be completed when the porosity reached 0.1 at any point. Their results showed that a certain optimum plate distance exists at which the cell capacity is highest.

A similar extension of the porous electrode models to a multi-layer cell was made by Tiedemann and Newman **[2].** Sunu [3] presented a one-dimensional model for a lead/acid cell consisting of a negative electrode, a porous separator, a reservoir of stagnant electrolyte and a positive electrode. The model was verified by comparison of the predicted and the experimentally measured cell voltages as a function of time for different discharge currents. White et al. **[4]** developed a model similar to that of Sunu, which was later extended to the starved and the hermetically sealed [5,6] lead/acid cell. Recently Bernardi et al. **[7]** have treated the two-dimensional case.

In the above papers, the models were mainly used for simulating galvanostatic discharge of the cell. Recently Maja et al. [8] presented a model that was also used for simulating fast charging of lead/acid batteries.

In this paper, a model has been derived for a lead/acid cell consisting only of a positive and a negative electrode mechanically compressed with a porous separator in between them. This cell design has proved

[1] Present address: Department of Chemistry, Trent University, Peterborough, Ont., **K9J** 7B8 Canada.

to yield a higher life under electric-vehicle conditions than the ordinary starter battery-type [9].

The previous models mentioned above use the transport equations for concentrated binary electrolytes. The rate equations for the charge-transfer processes are generally assumed to follow an ordinary Butler–Volmer equation, and the values of the kinetic parameters have generally not been critically evaluated or measured. The electrochemically active surface area is assumed to decrease linearly with the local extent of discharge according to a relation that does not take into account the strong influence of the current density on the active mass utilization. In the present paper a special emphasis has been put on using experimentally determined kinetic equations and relations for the influence of structural changes, as well as on the experimental validation of the model. A simple method for the numerical solution of the coupled differential equations for the different regions will also be presented.

2. Mathematical model

The cell investigated is schematically described in Fig. 1. It consists of a porous lead dioxide electrode, a porous negative lead electrode and a porous separator region between both electrodes. This cell design with no free electrolyte between the electrodes, which are compressed with separators in between them, is of interest for obtaining a long cycle life of the cell [9]. In both the electrodes the current is collected by a lead grid. In the cross section shown in Fig. 1 only two horizontal bars of the grid is shown in the positive electrode.

The basic assumptions underlying the model are essentially the same as in earlier papers (2–4). The separator is considered as completely saturated with the electrolyte solution. It is assumed that the sulfuric acid is completely dissociated into H^+ and HSO_4^- ions, respectively. The model equations can then be derived on the basis of the transport equations for a concentrated binary electrolyte given by Newman and Tiedemann [10], with the volume–average velocity taken as the reference velocity. Calculations using, e.g., Eq. (32) in Ref. 10, show that the convective term can actually be neglected in the acid balances; the decrease in porosity, due to the greater molar volume of lead sulfate than that of lead or lead dioxide, is to a great extent compensated by the decrease in electrolyte volume, due to the higher molar volume of sulfuric acid compared with water. The model equations for the three different regions are thus obtained by neglecting the convective term and applying Eqs. (8), (11), (12), (30) and (34) in Ref. [10]. The equations can be written in a dimensionless form by introducing the following dimensionless variables and parameters:

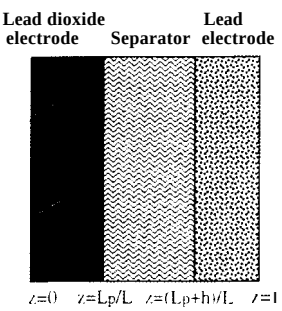

Fig. 1. Schematic drawing of the modelled cell showing the three different regions.

$$C = c/c_0$$

$$z = x/L$$

$$\eta' = \eta F/RT$$

$$i = i_2/I$$

$$\tau = tD_0/L^2$$

$$a = \kappa_0 RT/ILF$$

$$f = IL/2FD_0c_0$$

$$g = S_0 j_0^0 L/I$$

Transport parameters with index 0 denote free electrolyte conditions.

2.1. Positive electrode, $0 \leqslant z \leqslant L_p/L$

The electrode reaction during discharge is:

$$PbO_2(s) + 3H^+ + HSO_4^- + 2e^- \longrightarrow PbSO_4(s) + 2H_2O$$

The material balance for sulfuric acid in the pores of the lead dioxide electrode can be written:

$$\epsilon \frac{\partial C}{\partial \tau} = \frac{\partial}{\partial z}\left(\frac{D_{\text{eff}}}{D_0}\frac{\partial C}{\partial z}\right) + (3 - 2t_+^0 - (V_{\text{p,p}} - V_{\text{r,p}})c_0 C) f \frac{\partial i}{\partial z} - 2fi \frac{\mathrm{d}t_+^0}{\mathrm{d}C}\frac{\partial C}{\partial z} \quad (1)$$

The current balance is:

$$\frac{\partial}{\partial z}\left(a \frac{\kappa_{\text{eff}}}{\kappa_0}\frac{\partial \eta'}{\partial z}\right) + \frac{\partial}{\partial z}\left(a \frac{\kappa_{\text{eff}}}{\kappa_0}\left(3 - 2t_+^0 + 2\frac{c_0}{c_w}C\right)\frac{\mathrm{d}\ln(fc)}{\mathrm{d}C}\frac{\partial C}{\partial z}\right) = g_{\text{P}} \frac{S_{\text{P}}}{S_{0,\text{P}}}\frac{j}{j_{0,p}^0} \quad (2)$$

The local current density varies with the overpotential according to the following Butler–Volmer equation for the electrode kinetics:

$$j = j_{0,\text{P}}[\exp((2 - \alpha_c)\eta') - \exp(-\alpha_c \eta')] \quad (3)$$

where $j_{0,\text{P}}$ varies with the concentration.

2.2. Separator, $L_p/L < z < (L_p + h)/L$

The material balance is similar to that for the positive electrode but with no source term:

$$\epsilon \frac{\partial C}{\partial \tau} = \frac{\partial}{\partial z}\left(\frac{D_{\text{eff}}}{D_0}\frac{\partial C}{\partial z}\right) - 2f\frac{dt_+^0}{dC}\frac{\partial C}{\partial z} \quad (4)$$

The equation for the current density through the separator is:

$$\frac{\partial \phi}{\partial z} = (1-2t_+^0)\frac{d\ \ln(fc)}{dC}\frac{\partial C}{\partial z} - \frac{\kappa_0}{a\kappa_{\text{eff}}} \quad (5)$$

2.3. Negative electrode, $(L_p + h)/L < z < 1$

The electrode reaction in the negative electrode is:

$$Pb(s) + HSO_4^- \longrightarrow PbSO_4(s) + H^+ + 2e^-$$

The material balance is analogous to that for the positive electrode:

$$\epsilon \frac{\partial C}{\partial \tau} = \frac{\partial}{\partial z}\left(\frac{D_{\text{eff}}}{D_0}\frac{\partial C}{\partial z}\right) + (1-2t_+^0 + (V_{\text{p,n}} - V_{\text{r,n}})c_0 C)f\frac{\partial i}{\partial z} - 2fi\frac{dt_+^0}{dC}\frac{\partial C}{\partial z} \quad (6)$$

The current balance can be formulated as:

$$\frac{\partial}{\partial z}\left(a\frac{\kappa_{\text{eff}}}{\kappa_0}\frac{\partial \eta'}{\partial z}\right) + \frac{\partial}{\partial z}\left(a\frac{\kappa_{\text{eff}}}{\kappa_0}(1-2t_+^0)\frac{d\ \ln(fc)}{dC}\frac{\partial C}{\partial z}\right) = g_n\frac{S_n}{S_{0,n}}\frac{j}{j_{0,n}^0} \quad (7)$$

The rate of the electrochemical reaction is [11]:

$$j = j_{0,n}\frac{1-\exp(2\eta')}{\left(\frac{S_n j_0}{j_{\text{lim}}^c}\right)^0 - \exp(\alpha_c \eta')} \quad (8)$$

Although the notations for transport parameters, porosity and other parameters are the same for the different regions, their values are different in the different regions.

In the equations above, the electrolyte potential has been defined versus a hypothetical lead dioxide/lead sulfate reference electrode in the lead dioxide electrode and versus a lead/lead sulfate reference electrode in the separator and in the negative electrode. These different potentials are therefore defined only within their respective region. The total cell voltage can be calculated by means of Eq. (13), see below.

The following initial and boundary conditions can be formulated:

(i) for $t = 0$:

$$C = 1,\ X = 0,\ \epsilon = \epsilon_0 \quad \text{for } 0 \leqslant z \leqslant 1 \quad (9)$$

(ii) for $z = 0$ and $z = 1$:

$$\frac{\partial \eta'}{\partial z} = 0 \text{ and } \frac{\partial C}{\partial z} = 0 \quad (10)$$

(iii) for $z = L_p/L$:

$$D_{\text{eff}}^{\text{p}}\frac{\partial C}{\partial z} = D_{\text{eff}}^{\text{s}}\frac{\partial C}{\partial z}$$

and,

$$\frac{\partial \eta_s'}{\partial z} = \frac{\kappa_0}{a\kappa_{\text{eff}}} - \left(3 - 2t_+^0 + 2\frac{c_0}{c_w}C\right)\frac{d\ \ln(fc)}{dC}\frac{\partial C}{\partial z} \quad (11)$$

(iv) for $z = (L_p + H)/L$:

$$D_{\text{eff}}^{\text{s}}\frac{\partial C}{\partial z} = D_{\text{eff}}^{\text{n}}\frac{\partial C}{\partial z}$$

and,

$$\frac{\partial \eta_s'}{\partial z} = \frac{\kappa_0}{a\kappa_{\text{eff}}} - (1-2t_+^0)\frac{d\ \ln(fc)}{dC}\frac{\partial C}{\partial z} \quad (12)$$

In addition, the condition that the concentration is a continuous function throughout the cell has been used. The boundary conditions in Eqs. (11) and (12) connect the concentration profiles in the three different regions. The cell voltage can be calculated by means of the following equation:

$$E_{\text{cell}} = E_{\text{cell}}^{\text{eq}}(C(L_p)) + \frac{RT}{F} \times [\eta(L_p) - \eta(L_p + h) + \phi(L_p) - \phi(L_p + h)] \quad (13)$$

where $E_{\text{cell}}^{\text{eq}}(C)$ is the equilibrium cell voltage at concentration C. This value can be found in reference tables. The approximate polynomial function formulated by White and co-workers [5] has been used in this work.

The effects of structural changes have been taken into account by means of the parameter X, the degree of discharge:

$$X_i = \frac{IL}{D_0 q_{0,i}}\int_0^\tau \frac{\partial i}{\partial z}\,d\tau \quad (14)$$

The varying porosity in the porous electrodes can be calculated as a function of X:

$$\epsilon = \epsilon_{0,i} - k_i(1-\epsilon_{0,i})X_i \quad (15)$$

Effective transport parameters are assumed to vary according to the following relationship, written for the effective conductivity as an example:

$$\kappa_{\text{eff}} = \lambda_i\left(\frac{\epsilon}{\epsilon_{0,i}}\right)^{1.5}\kappa(C) \quad (16)$$

where λ_i is the ratio between the effective conductivity in the active mass in its fully charged state and the conductivity in free electrolyte. $\kappa(C)$ is the conductivity of the free electrolyte at concentration C. A similar relation can be formulated for the effective diffusivity.

The active surface area decreases during discharge according to a relation that has borrowed its essential features from the empirical Peukert equation [11]:

$$S_i = S_{0,i}\left(1 - \frac{I^n}{K'_{a,i}}\int_0^\tau \left(\frac{\partial i}{\partial z}\right)^n \mathrm{d}\tau\right) \quad (17)$$

This relation takes into account the important fact that the electrode surface will be covered more rapidly with smaller lead sulfate crystals when the current density is higher.

3. Influence of the grid and its shape

The presence of the current-collecting grid is difficult to take into account in the model. The grid occupies about 15 to 20% of the volume of the electrode. Furthermore, the shape of the grid is such that its fraction ϵ_g of the vertical cross section varies linearly from zero at the exterior surface to a maximum at the midplane of the electrode, see Fig. 1. An exact analysis would require a two-dimensional treatment. Here two different simplified approaches will be made, both leading to a one-dimensional analysis.

In the first case, the grid cross section is taken to be rectangular, constituting a constant fraction of the plate cross section, so that the problem becomes a truly one-dimensional one. The true geometric current density and effective transport parameters have to be calculated from the values measured with respect to the total geometric area including the grid by dividing them by the factor $(1-\epsilon_g)$, where ϵ_g is the average fraction of the vertical cross section that the lead grid occupies. In this case the theoretical charge output per unit volume of active mass should be written:

$$q_i = 2F\frac{\rho_i}{M_i}(1-\epsilon_{0,i}) \quad (18)$$

In the second case, the macrohomogeneous approach is extended to include also the grid material in such a way that the total effective porosity in terms of electrolyte volume per electrode volume on the left-hand side in the acid balances is written:

$$\epsilon = \epsilon_m(1-\epsilon_g) \quad (19)$$

where ϵ_m is the porosity of the active material. For the two different electrodes ϵ_g varies according to the following relations:

(i) $0 \leqslant z \leqslant L_p/2L$:

Table 1
Values of the parameters used in the calculations; temperature= 23 °C

Parameter	Value or expression	Ref.
c_0	5.0 mol dm^{-3}	
D_0	2.9×10^{-9} m^2 s^{-1}	[4]
D_c/D_0	$0.706+0.294C$	[14]
k_i	$(V_p - V_r)/V_{r,i}$	
L_p	1.9 mm	measured
L_n	1.7 mm	measured
L	7.0 mm	measured
$\frac{\mathrm{d}\ln(fc)}{\mathrm{d}C}$ [a]	$\frac{4.4763f_1 + 9.605f_2}{(f_1 - f_2)}$	[12]
t^0_+	$0.8224 - 0.0725C - 0.0302C^2$ or different constant values	
$S_0 j^0_0$	25200 (p), 1.9×10^5 (n) A m^{-3}	[13,11]
j^s_{lim}	-1×10^5 A m^{-3}	[11]
$V_{p,p}$, $V_{p,n}$	48.9×10^{-3} m^3 kmol^{-1}	[14]
$V_{r,p}$	25.5×10^{-3} m^3 kmol^{-1}	[14]
$V_{r,n}$	18.3×10^{-3} m^3 kmol^{-1}	[14]
λ_p	0.19	[13]
λ_n	0.33	[11]
λ_s	varies according to Figures	
n	1.35 (p), 1.4 (n)	
α_c	1.5 (p), 0.9 (n)	[13,11]
ϵ_g	0.17 (average)	measured
ϵ_0	0.55–0.58 (p), 0.60-0.66 (n)	measured
κ_0	76 Ω^{-1}	[4]
κ	$\kappa_0(0.20 + 2.1C - 1.3C^2)$ $(0.2 \leqslant C \leqslant 1)$	[14]
	$\kappa_0 2.84C$ $(0 \leqslant C < 0.2)$	

[a] Where $f_1 = 0.07941\exp(2.9842C)$ and $f_2 = 0.06645\exp(-6.4033C)$.

$$\epsilon_g = 4\bar{\epsilon}_g z\frac{L}{L_p} \quad (20)$$

(ii) $L_p/2L \leqslant z \leqslant L_p/L$:

$$\epsilon_g = 4\bar{\epsilon}_g\left(1 - z\frac{L}{L_p}\right) \quad (21)$$

(iii) $(L_p+h)/L \leqslant z \leqslant (L_p+h+L_n/2)/L$:

$$\epsilon_g = 4\bar{\epsilon}_g\left(z - \frac{L_p+h}{L}\right)\frac{L}{L_n} \quad (22)$$

(iv) $(L_p+h+L_n/2)/L \leqslant z \leqslant 1$:

$$\epsilon_g = 4\bar{\epsilon}_g\left[1 - \left(z - \frac{L_p+h}{L}\right)\frac{L}{L_n}\right] \quad (23)$$

The geometric current density and mass fluxes are defined with respect to the total cross-sectional area, including the grid.

The transport parameters must in this case be modified according to the following relation for the effective diffusion coefficient, compare with Eq. (16):

$$D_{eff} = \lambda_i\left(\frac{\epsilon}{\epsilon_{0,i}}\right)^{1.5}(1-\epsilon_g)D(C) \quad (24)$$

The theoretical charge output per unit electrode volume and the initial active surface area also vary along the depth of the electrode:

$$q_i = 2F \frac{\rho_i}{M_i} (1 - \epsilon_{0,i})(1 - \epsilon_g) \quad (25)$$

$$S_{0,i} = S^0_{0,i}(1 - \epsilon_g) \quad (26)$$

Input parameters are given in Table 1. Values of the transport parameters in free electrolyte have been taken from data in the literature. The mean activity coefficient for the sulfuric acid dissociated as a binary electrolyte, has been calculated from a correlation of data for the mean activity coefficient of hydrogen and sulfate ions at complete dissociation of sulfuric acid [12]. The conductivity and diffusivity of 5.0 M sulfuric acid were taken from values given for 25 °C in Ref. [1], which were recalculated to 23 °C using the equations for temperature dependence for these parameters given in the same paper.

Kinetic parameters for the lead and lead dioxide electrodes were taken from Refs. [11] and [13] respectively. In the latter work fitted values of the cathodic charge-transfer coefficient varied around 1.5. Using instead a value of 2, as found for other lead dioxide electrodes used in previous works [14,15] did not significantly change the results.

4. Numerical procedure

The system of non-linear differential equations was solved by means of the finite difference method. Within each region (positive electrode, separator and negative electrode, respectively) a uniform grid was chosen. The first derivative $\partial C/\partial z$ in the grid point with number i was approximated as $(C_{i+}, - C_{i-1})/(2\ \mathrm{Ah})$, where Ah is the step length. This gives a second-order approximation of the first derivatives. The second derivatives like, for example, the first term on the right-hand side of Eq. (1), cannot be approximated that easily. The reason for this is that the effective diffusion coefficient depends also on concentration and porosity, i.e., varies with the coordinate z. Therefore, the finite difference approximation at the point with number i can be taken in the form:

$$\frac{\partial}{\partial z}\left(D \frac{\partial C}{\partial z}\right)_i = \left(D_{i+1/2} \frac{C_{i+1} - C_i}{\Delta h} - D_{i-1/2} \frac{C_i - C_{i-1}}{\Delta h}\right)/\Delta h \quad (27)$$

The value of the diffusion coefficient at the point (i+ 112) is calculated in terms of the value of concentration at this point, $C_{i+1/2}$, which can be estimated as $(C_{i+1} + C_i)/2$. The value of the porosity in a point between two mesh points is calculated in a similar way. Eq. (27) gives an approximation with a precision of somewhat less than second order, depending on how significantly the diffusion coefficient varies.

The first-order accuracy implicit stepping technique has been used for discretization of the time derivatives. The approximation of boundary conditions is very i m portant. It is well known that the boundary condition $\partial C \partial z = 0$, written in the simplest form:

$$C_1 - C_0 = 0 \quad (28)$$

gives only a first-order accuracy, which would make the second-order approximation for the differential equation lose its attraction. White [5,6,16] proposed to use a three-point approximation for each of the first derivatives at the boundary between two regions. This gives an equation for the boundary condition that involves five mesh points. An algorithm for solving such a problem was proposed in Ref. [17].

In this work we used instead the approximation of the boundary condition which is standard in fluid dynamic numerical works. The mesh grid was shifted so that all boundaries were half way between two grid points, and imaginary points were added at a half step outside the regions. In this case, Eq. (28), where now i=O corresponds to an imaginary point, has second-order accuracy.

For the boundary, the value of the effective diffusion coefficient was taken as the harmonic mean value of the values of the effective diffusion coefficient in the neighbouring grid points in the electrode(e) and separator(~),respectively:

$$D_{\mathrm{eff}} = \frac{2 D_{\mathrm{eff,e}} D_{\mathrm{eff,s}}}{D_{\mathrm{eff,e}} + D_{\mathrm{eff,s}}} \quad (29)$$

The same procedure can be used for the equations for the electric potential, Eqs. (2) and (7). No interface conditions for the concentration are required. Three equations for the concentration in the three different regions, Eqs. (1), (4) and (6), are, in fact, made into one quasi-linear equation with variable coefficients. On the boundaries of the separator these coefficients change stepwise, but from physical and numerical points of view it remains the same equation. In this way we get a standard tridiagonal matrix for the full system, independently of the number of the inner boundaries.

The algorithm used for solving the discretized equations is described below:

(i) Eq. (2) for the potential within the positive electrode with boundary conditions given in Eqs. (10a) and (1lb) was linearized and solved by an over-relaxation procedure. For the solution of implicit space derivatives a simple Thomson algorithm was used. In order to have a stable convergence from arbitrary 'initial' values, an artificial viscosity term was added. At the end of this stage two conditions were checked: (i) a stable potential profile has been obtained, and (ii) the boundary

conditions given in Eqs. (10a) and (11b) for the full equations (not only for the linearized) have been fulfilled with sufficient accuracy (about 10^{-8}).

(ii) The changes in porosity and active surface at this potential distribution is calculated from Eqs. (14) to (17). The new values of porosity requires a correction of the potential profile, i.e., returning to the step (1). Then we can correct porosity one more time. The procedure according to the steps (1) to (2) converged very fast, it took only 2 to 3 iterations.

(iii), (iv) An analogous procedure for the potential and porosity distributions within the negative electrode must be done. Note, that we do not solve the equation for the potential in the separator. Eq. (5) for the potential distribution can be integrated with respect to the coordinate. Therefore, if we know the concentration profile within the separator, we can find the potential distribution immediately.

(v) The overvoltage and porosity profiles, obtained in steps (i) to (iv) were substituted into the equation for concentration. The single equation for the complete multi-region system was used. This equation has also non-linear factors, depending upon the concentration. Therefore, an iteration procedure is necessary. After calculations of new values of concentration, the new potential distribution was calculated from steps (i) and (iii) and then porosity corrections were made, steps (ii) and (iv).

The main convergence loop including steps (i) to (v) gives in general good results already after two or three iterations, but in some complicated cases, for example, at the end of discharge, when a region with low concentration appears, the number of iterations can grow significantly.

At the end of procedure (i) to (v), we obtained the solution of the non-linearized system on the next time step, using implicit time-derivative technique. After that, the next time step can be taken.

The main advantages of this algorithm are:

(i) It is absolutely stable, it converged for any time step and length coordinate step, as well as for small values of the concentration. In the case when convergence becomes bad, the program automatically reduces the time step. It gives a possibility to calculate up to very high degrees of discharge when other algorithms tried could not work.

(ii) It gives us the possibility to check the accuracy of the calculations of each component separately and of the system as a whole.

(iii) At the same time, we do not loose the attractive feature of the Thomson algorithm, namely linearity; the calculation time is proportional to the number of grid points (rather than to the square of this number).

(iv) A discretization of a second-order accuracy was used for the equations as well as the interface and boundary conditions.

The execution time on a personal computer is several minutes, which allows us to observe the system evolution directly on the screen.

Further details about the stability and conservative properties of the numerical method are given in the Appendix.

5. Experimental

The electrodes used in this study were pasted electrodes for commercially available SLI-batteries manufactured by Tudor **AB** at Nol, Sweden. The full size dimensions were 115 mm x 155 mm with a thicknesses of approximately 1.7 and 1.9 mm for the lead and the lead dioxide electrodes, respectively. The current-collector grids were made of a lead alloy with 2.5% Sb. The experiments were performed on electrode samples that had been cut from the full size plates to about 51 mm in height and 34 mm in width. The samples were taken both from the upper and the lower parts of the plates, so that one side of each electrode sample consisted of the grid bar to which a 3 mm lead rod was welded as the current collector.

The electrolyte used during the preparative cycling and before discharge experiments was in all cases 5.05 M sulfuric acid prepared from 98% sulfuric acid (Merck, pro analysi) and purified water from a combined Milli-RO 15 and Milli-Q water purification system from Millipore. The concentrations were determined by acid–base titrations and/or refractive index measurements.

Lead and lead dioxide electrodes were precycled in pairs in glass beakers; the electrodes were separated by a microporous separator to avoid short-circuiting. The electrodes were allowed to soak in the electrolyte for about 1 h before they were automatically cycled at a constant-current density of 100 A m^{-2} according to the following scheme:

1. charge to oxygen evolution;
2. rest for 3600 s;
3. discharge for 14605 s, corresponding to approximately 80% depth-of-discharge at rated capacity of the cell;
4. rest for 3600 s;
5. recharge for 17 526 s, corresponding to 20% overcharge, and
6. steps 2 to 5 were repeated in total three times.

After the preparative cycling, the electrolyte, in the beakers, was changed to ensure a concentration of 5.05 M. The beakers, with electrolyte and electrodes, were placed under vacuum maintained by a water jet for a period of at least 10 h. In order to remove as much as possible of the gas in the porous electrodes and to replace the gas with the electrolyte. After evacuation, the electrolyte was changed once again. The temperature during the discharge experiments was kept at 23 °C.

The so-prepared electrodes were mounted into an experimental cell of which a schematic drawing is given in Fig. 2. The cell consisted of two thick endplates made of poly(tetrafluoroethylene) (PTFE) with a U-formed distance made of poly(methyl methacrylate) (PMMA) forming a well-defined cell. The total distance over the electrodes was 7.0 mm. The height and the width of the cell matched the form and dimensions of the electrodes. In each endblock there was a hole perpendicular to the electrode surface. The hole was used to measure, via a capillary, the electrode potential at the rear of each electrode by Hg/Hg_2SO_4 reference electrodes in saturated K_2SO_4 manufactured by Radiometer. Three glass-fibre separators (BG 200 17 by Hollingsworth and Vose), with the same dimensions as the electrodes, were placed between the electrodes. The separators were immersed in sulfuric acid and evacuated in the same way as the electrodes. A mechanical pressure was applied perpendicularly to the electrode plates to seal the cell and to get a well-defined electrode distance. Any free acid, i.e., acid that was not soaked by the electrodes or the separator, was removed from the cell container with a syringe. This setup defined the cell at time equal to zero.

The cell was then galvanostatically discharged at different current densities varying from 100 to 1000 A m^{-2}. During discharge, the cell voltage and the electrode potentials at the rear of the electrodes were measured on x–t recorders. The discharge was stopped at a cell voltage of 1.0 V. The cell was then immediately disassembled. The remaining amount of sulfuric acid was then separately leached out from each cell component by soaking in multiple small portions of purified water until the leaching water was neutral. The amount of acid in each cell component could then be determined by an acid–base titration. Some cells were disassembled without discharge in order to determine the amount of acid and thereby the effective porosity of the electrodes and the separators. The concentration profiles in the cells after discharge could thus be calculated from the remaining amount of acid according to the titrations as well as the final porosity which, for the two electrodes, could be calculated from the initial porosity and the change in porosity due to the formation of lead sulfate from lead and lead dioxide, respectively.

The distribution of lead sulfate along the thickness of the electrodes was determined with an electron-probe microanalyser (ARL SEMQ 42) by recording the S Kα radiation. The electrodes for the sulfate analyses were leached in acetone instead of water. The electrodes were then dried at 50 °C and representative samples from the central part of the electrodes were taken out. The samples were then moulded into an epoxy resin under vacuum, polished with diamond paste and sputtered with a conductive layer of carbon before analysis.

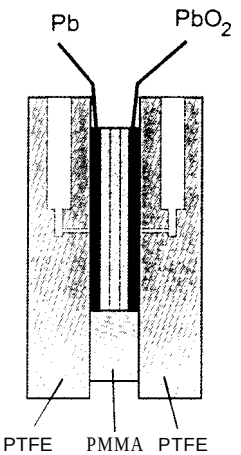

Fig. 2. Schematic drawing of the cell used in the discharge experiments

6. Results and discussion

6.1. Effects of different parameters

The computer program was first tested with the model equations and input parameters used by Nguyen and White in Ref. [16]. The results obtained were in good agreement with those of Fig. 2 in that work. Similar results obtained with the model and input parameters used in this work are shown in Fig. 3 for a current density of 1000 A m^{-2}. This Figure shows that the discharge capacity at a high rate of discharge is mainly determined by an acid depletion in the positive electrode.

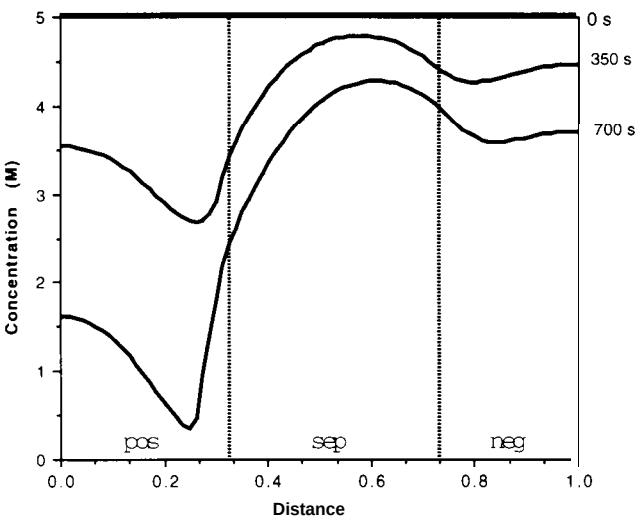

Fig. 3. Model predictions of the changes in sulfuric acid concentration in a cell at a discharge with 1000 A m^{-2}. Constant t_+^0 =0.79. Porosity of positive plate = 0.58, of negative plate = 0.66, and of separator = 0.53. Thickness of positive plate=2.15 mm, of negative plate= 1.8 mm, and of separator region = 2.4 mm. $K_a' = 15 \times 10^7$ (A m^{-2})$^{1.35}$ s for both electrodes.

In these calculations a constant value of the transference number was used. It turned out that calculations with a varying transference number did not give concentration profiles that were in agreement with the acid conservativity condition. The calculated consumption of sulfuric acid could deviate by up to 10% from the value calculated by means of an overall acid balance using Faraday's law. All subsequent calculations were therefore performed with a constant transference number.

Initial calculations showed that the shape of the grid that was assumed in the model did not affect the results significantly. The main difference was that the porosity profiles calculated by means of using Eqs. (20) to (23) exhibited a slight maximum in the interior of the electrode, see Fig. 5. The calculations reported here were performed using Eqs. (20) to (23).

The effects of the parameters K'_a and n are shown in Figs. 4 and 5. When $n = 1$ and the maximum possible utilization of the active electrode material is equal to the theoretical value, then mainly the outer layer of the electrode has been discharged and the local degree of discharge has its maximum at the outer surface of the electrode. With $n = 1.35$ and a value of K'_a, which corresponds to a maximum degree of utilization that is lower than the theoretical one, the maximum of the current-density distribution moves progressively inwards as the outer layers of the electrode are de-activated by the formed lead sulfate. At a constant value of n a larger value of K'_a means in general a higher possible utilization of the active electrode material and, therefore, a higher discharge capacity. A lower value of K'_a for the positive electrode forces the reaction deeper into the interior of the electrode due to a more rapid de-activation of the parts of the electrode that are close to the interface. For $n > 1$, the high initial current density in the outermost layer of the electrode causes the electrode material in this layer to become de-activated at a relatively low degree of discharge. The degree of discharge therefore has a maximum at some distance from the interface between the electrode and the separator. This is clearly pronounced for $K'_a = 7 \times 10^7$ $(A\ m^{-2})^{1.35}$ s for the positive electrode in Fig. 5. This shape of the curve for the degree of discharge is in better agreement with the distributions of formed lead sulfate measured with electron-probe microanalysis. It was found that a reasonable value of K'_a lies in the region of $(7–15) \times 10^7$ $(A\ m^{-2})^{1.35}$ s for the positive electrode. In this region the discharge is mainly limited by an acid depletion in the positive electrode.

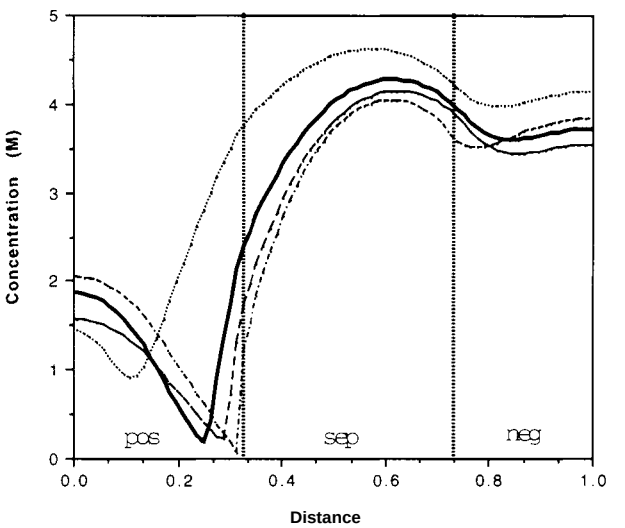

Fig. 4. Predicted concentration profiles for different values of K'_a for the positive electrode: (dotted line) $K'_a = 3 \times 10^7$ $(A\ m^{-2})^{1.35}$ s; (bold, solid line) $K'_a = 7 \times 10^7$ $(A\ m^{-2})^{1.35}$ s and (dashed line) $K'_a = 20 \times 10^7$ $(A\ m^{-2})^{1.35}$ s. Other data as in Fig. 3. Dot-dashed line for $n = 1$ instead of 1.35 and only theoretical limitation of the local degree of discharge. Discharge time=472, 700, 750 and 760 s, respectively.

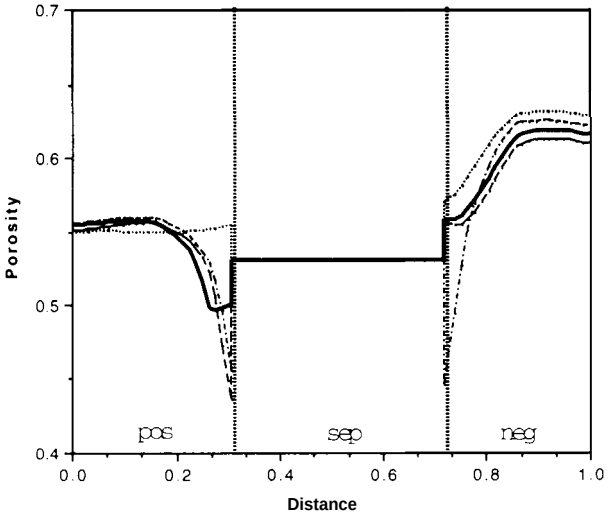

Fig. 5. Model predictions of the changes in porosity for the different cases in Fig. 4.

In contrast, for the lowest value of K'_a used in Figs. 4 and 5, the maximum local mass utilization is very low and the discharge capacity becomes unrealistically low. Figs. 4 and 5 show that in this case the discharge capacity would be limited by the low (and fairly uniform) active mass utilization.

Fig. 6 shows the effect of the separator porosity on the discharge capacity at a high rate discharge (1000 $A\ m^{-2}$). It can be seen that this parameter has a rather weak influence on the discharge capacity, although at given dimensions of the different regions a higher separator porosity means both a higher effective diffusivity and a larger amount of the stored acid. The explanation for this weak dependence at high rates of discharge is that mainly the acid in the pores of the electrode is being consumed in the electrode reactions during the relatively short discharge process, which is terminated by the depletion of sulfuric acid in a zone

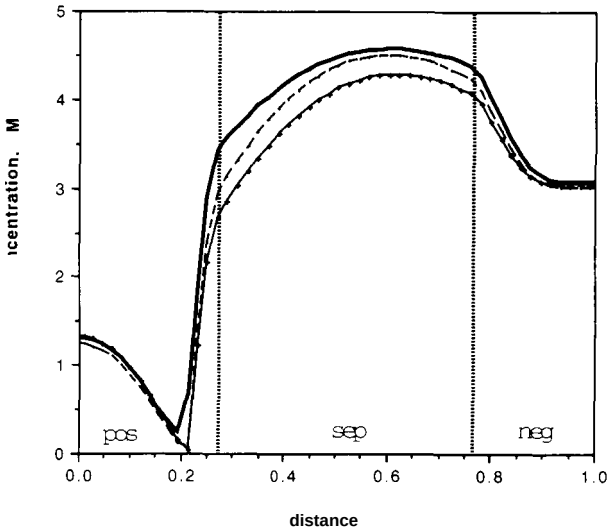

Fig. 6. Predicted concentration profiles for different values of the separator porosity: (solid line) 0.96, (dashed line) 0.7 and (lower line) 0.5. λ_s for the separator was taken as $\epsilon^{1.5}$. Constant $t^0_+ = 0.79$. $K'_a = 15 \times 10^7$ for both electrodes. Discharge time = 724, 719 and 699 s, respectively.

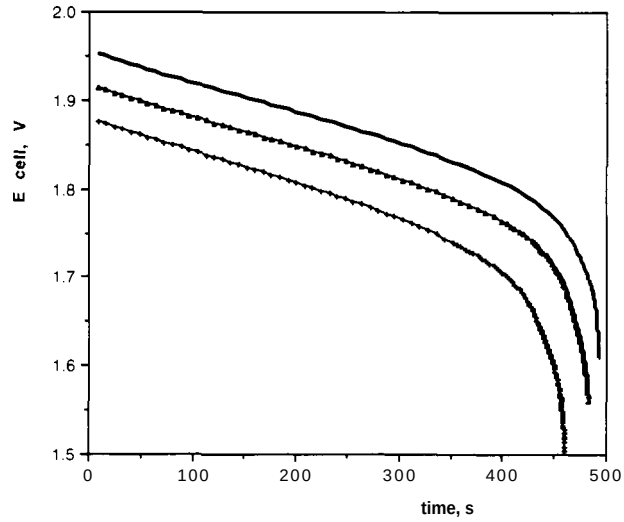

Fig. 7. Predicted voltage–time curves for a cell with 1.0 mm thick electrode and different thicknesses of the separator: (upper line) 1 mm, (line in between) 2 mm, and (lower line) 3 mm. Current density=lOOO A m^{-2}. $K'_a = 10 \times 10^7$ (A m^{-2})$^{1.35}$ s for the positive electrode and $K'_a = 15 \times 10^7$ (A m^{-2})$^{1.4}$ for the negative electrode. Porosity of separator =0.804. λ_s for the separator =0.33. Porosity of negative electrode =0.66. $t^0_+ = 0.79$.

just behind the de-activated outer layer of the positive electrode.

For low rates of discharge, when the discharge capacity is higher and the consumption rate of sulfuric acid in the electrodes can more easily be balanced by the transport rate of acid from the separator into the electrodes, a high separator porosity has a much more positive influence.

A similar dependence holds for the discharge capacity as a function of the thickness of the separator. Figs. 7 and 8 show discharge curves for a cell with 1.0 mm thick electrodes and with separators of different thicknesses. At a high rate of discharge (Fig. 7) the discharge capacity is fairly independent of the separator thickness. Surprisingly, the discharge capacity is even larger for the thinner separator. This can, at least partly, be explained by the higher ohmic potential drop in the thicker separator.

For a lower rate of discharge (Fig. 8) the discharge capacity increases with the separator thickness, since the acid in the pores of the separator is consumed to a higher extent in thiscase. At the beginning of discharge, the cell voltage is the highest for the thinnest separator, due to a lower ohmic potential drop across the separator, while the relation is reversed with time when the overall depletion of sulfuric acid becomes determining.

In order to have a sufficiently large amount of electrolyte in the case low rate discharges, the separator region must therefore be made sufficiently thick and/or must have a sufficiently high porosity.

6.2. Comparison with experimental results

An important aim of this study was to validate the model by comparing results predicted by the model

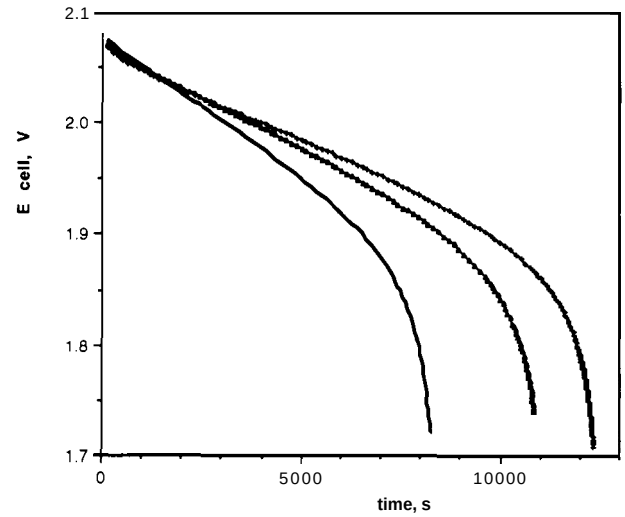

Fig. 8. As in Fig. 7 but at a discharge current density of 100 A m^{-2}.

with those obtained experimentally. Although the electrodes did not differ very much with respect to measured porosity and geometric dimensions, and the preparative cycling was the same, the discharge capacity varied unexpectedly much. This is shown in Fig. 9, in which calculated and measured concentration profiles at a high current density, 490 A m^{-2}, are compared. The experimental discharge capacity in four different experiments varied between 2121 and 2548 s. The calculated discharge time of 2012 s is in good agreement with the lowest value obtained experimentally, which, on the other hand, is 8% lower than the average and 17% lower than the highest discharge time obtained

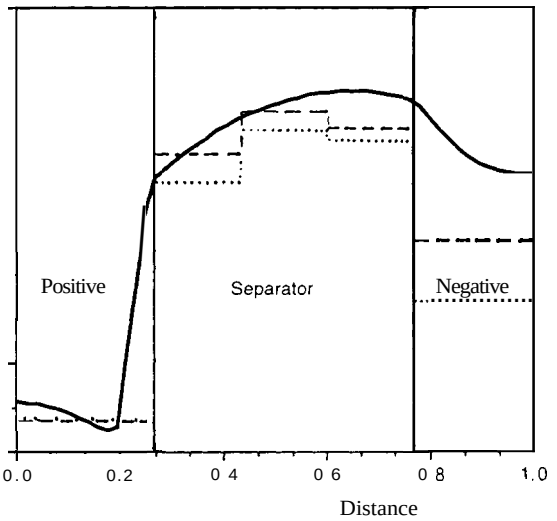

Fig. 9. Comparison of the (solid lines) predicted and (dashed lines) measured concentration profiles at a discharge with 490 A m^{-2}. $t^0_+ = 0.81$. Assumed porosity of negative electrode = 0.60, of positive electrode = 0.58. Porosity of separator = 0.96. A, for the separator = 0.90. Predicted discharge time = 2012 s. Experimental discharge time = 2121 (dashed lines), and 2548 s (dotted lines).

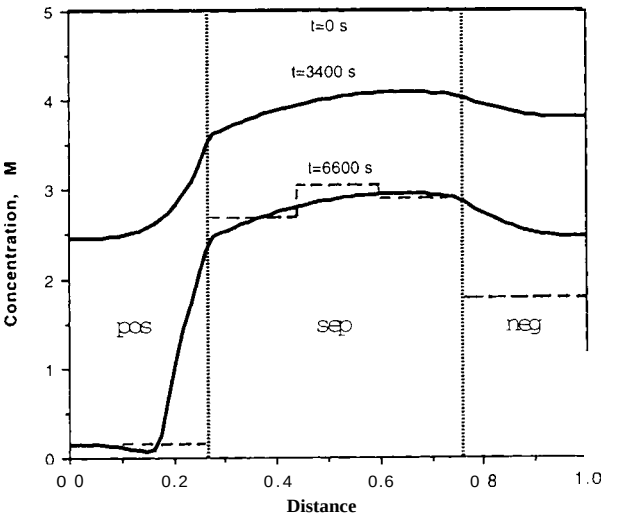

Fig. 10. Comparison of the (solid lines) predicted and (dashed lines) measured concentration profiles at a discharge with 200 A m^{-2}. Other input data as in Fig. 9. Predicted discharge time=6600 s. Experimental discharge time = 6942 s.

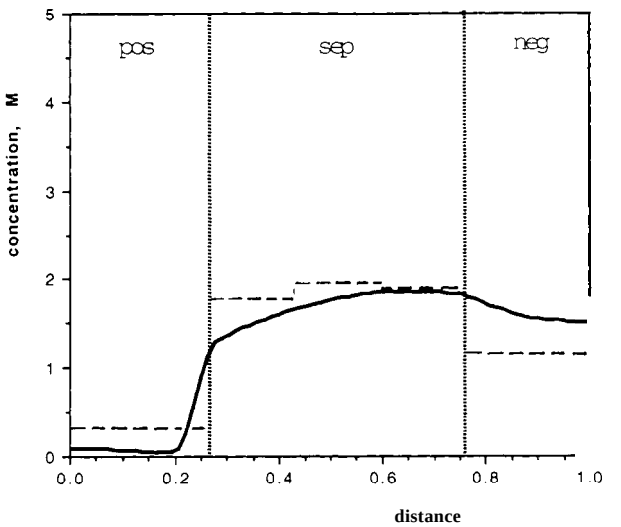

Fig. 11. Comparison of (solid lines) predicted and (dashed lines) measured concentration profiles at a discharge with 100 A m^{-2}. Other input data as in Fig. 9. Predicted discharge time = 17600 s. Experimental discharge time = 17310 s.

experimentally. The measured concentration profiles are in fair agreement with those predicted by the model. Both the experiments and the theory show that the discharge capacity at high discharge rates is limited by an acid depletion in the positive electrode.

Similar results were obtained for a current density of 1000 A m^{-2}. According to the model predictions in Figs. 3 and 4, the discharge time would be around 700 to 750 s, whereas the experimental results give discharge times varying between 830 and 940 s.

For 200 A m^{-2} (Fig. 10), the model predicts, with input parameters valid for room temperature, a discharge time that is 4 to 7% lower than that obtained experimentally. The predicted discharge time for 100 A m^{-2} (17 600 s) (Fig. 11) is in good agreement with the experimentally measured discharge time of 16 620-17 970 s. The measured concentrations in the separator are somewhat higher than the predicted values, whereas, on the other hand, the measured concentration in the negative electrode is again significantly lower than the calculated value.

Figs. 9 to 11 show, that in comparison with the experimental results, the model generally predicts a somewhat too rapid depletion of sulfuric acid, especially at high rates of discharge, and a too low decrease in sulfuric acid concentration in the negative electrode. A common cause for these two discrepancies should first be searched for. One parameter that affects the resulting distribution of acid between the different regions is the transference number. According to Eqs. (1) and (6) a higher value of the transference number gives a slower consumption rate of sulfuric acid in the positive electrode and a higher consumption rate in the negative. It should be kept in mind that the value of this parameter for the volume–average velocity as the reference velocity (as in this case) has somewhat arbitrarily been set equal to the transference number with respect to the solvent velocity [10]. According to the derivation of the transport equation with volume–average velocity as reference velocity:

$$t_+ = (1 - c_+ V_+) t^0_+ + c_- V_- t^0_- \tag{30}$$

where $c_+ V_+$ and $c_- V_-$ cannot be determined individually. Newman has, therefore, arbitrarily put $t^0_+ \nu_+ V_+ = t^0_- \nu_- V_-$, which gives $t_+ = t^0_+$. This relation has been used in our model. Now, assuming instead that the molar volume of $H^+ \approx 0$, which seems not too

unrealistic, considering the size of a proton. This also means that $c\_V\_ \approx cV_e$, and we obtain:

$$t_+ = (1 - cV_e)t_+^0 + cV_e \quad (31)$$

Using known data it can be shown that t_+ estimated from Eq. (31) is only 1% higher than t_+^0 for a 1 M sulfuric acid solution, whereas it is 8% higher for a 5 M sulfuric acid solution.

Fig. 12 shows the effect of the transference number on the resulting concentration profile. As anticipated, the obtained concentration profile in the cell is in better agreement with the experimental results when the value of the transference number is increased. However, an unreasonably high value would be needed to give the low concentrations in the negative electrode measured experimentally.

There are, therefore, probably different causes for the discrepancies between model predictions and experimental results for the two different electrodes. In order to simulate correctly the behaviour of the positive electrode at high rates of discharge significantly higher values of the transport parameters are required. These higher values could be a result of an increased temperature in the electrode due to irreversible losses at the relatively high overpotentials. This would also explain the increasing discrepancy between theoretical and experimental results with increasing current density, since the thermal effects are larger at higher current densities. If the thermal effects cause the unexpectedly high discharge times at higher current densities, then it is also reasonable that the agreement should be better at lower discharge rates when these thermal effects are smaller. A rough estimation of the adiabatic temperature rise in the cell using data from Ref. [18] gives an average value of 3–5 °C after discharge with 500–1000 A m^{-2}. These values are not sufficiently high to explain the discrepancies for the positive electrode, but due to the highly non-uniform current and potential distributions in this electrode, the temperature may rise to much higher values locally in the critical interface region between the separator and the positive electrode. Already, the Joulean heat production rate in the outer layer of the positive electrode, in which the effective conductivity of the electrolyte is low due to a low porosity and a decreasing acid concentration, can be estimated to be considerably higher than the average. In order to investigate the thermal effects further, a non-isothermal model incorporating energy balances is required.

Temperature effects do not explain the opposite deviation in the negative electrode, in which the measured sulfuric acid concentration is significantly lower than the calculated value. It should be stressed that the calculations have been performed with the lowest measured value of the porosity of the negative plates. It is, therefore, not very likely that the real porosity is actually somewhat lower, which would otherwise explain the deviations. The microprobe analyses of the sulfur distribution in the negative electrode after discharge show that the overall utilization of the negative active material is fairly uniform, whereas the model predicts a non-uniform distribution with a higher degree of discharge in those parts closer to the electrolyte matrix. This may, at least partially, explain why the model predicts an average concentration in the negative that is higher than the measured values.

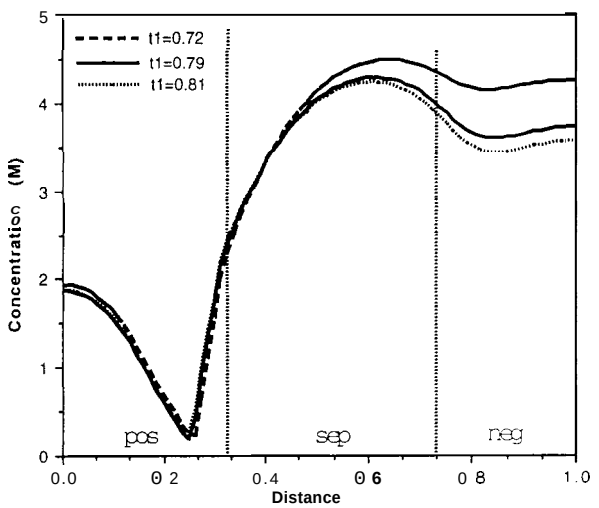

Fig. 12. Predicted concentration profiles at different transference numbers for the hydrogen ion: (upper curve) 0.72, **(middle curve)** 0.79 **and (lower curve)** 0.81. **Predicted discharge time = 638,** 700 **and** 715 **s, respectively. Other data as in Fig. 3 but with** $K_a' = 10 \times 10^7$ **(A** $m^{-2})^{1.35}$ **s for the positive electrode.**

7. Conclusions

1. Both the theoretical and the experimental results show that the discharge capacity is limited by the acid depletion in the positive electrode for current densities between 100 and 1000 A m^{-2}.

2. At high rates of discharge, the amount of sulfuric acid in the pores of the separator does not affect the discharge capacity to any greater extent. At lower discharge rates, on the other hand, the discharge capacity increases strongly with an increasing amount of electrolyte in the separator.

3. The model can be used for optimizing the geometric dimensions of the positive and negative electrodes and the separator in the lead/acid battery for different applications.

4. Experimental and theoretical results are in good agreement at medium to low current densities, whereas the model predicts a somewhat too low discharge capacity at high current densities, possibly because it does not take into account the thermal effects.

5. Further investigations are required to explain the discrepancies between the model predictions and the experimental results for the decrease in the sulfuric acid concentration in the negative electrode during discharge.

8. List of symbols

a	$\kappa_0 RT/ILF$
c	concentration of sulfuric acid (mol dm^{-3})
C	dimensionless concentration of sulfuric acid
D	diffusion coefficient of sulfuric acid (m^2 s^{-1})
E_{cell}	cell voltage (V)
f	$IL/2FD_0c_0$
f	activity coefficient in Eqs. (2), (7), (11) and (12)
F	Faraday constant (96 487 A s mol^{-1})
g	$S_0 j_0^0 L/I$
h	thickness of separator region (m)
i	dimensionless current density in the pore electrolyte
i_2	current density in the pore electrolyte (A m^{-2})
I	geometric current density (A m^{-2})
j	local true current density (A m^{-2})
j_{lim}^c	cathodic limiting current density (A m^{-2})
j_0	exchange-current density (A m^{-2})
k_i	$(V_{p,i} - V_{r,i})/V_{r,i}$
$K'_{a,i}$	constant defined by Eq. (17)
L	thickness (m)
M	molecular weight (kg mol^{-1})
n	exponent defined by Eq. (17)
$q_{0,i}$	charge corresponding to the initial amount of i (A s m^{-3})
R	universal gas constant (8.3143 J mol^{-1} K^{-1})
S	specific active surface area (m^{-1})
t	discharge time (s)
t_+^0	transference number of hydrogen ion for solvent velocity as reference velocity
t_r	transference number of hydrogen ion for volume–average velocity as reference velocity
T	absolute temperature (K)
V_+	molar volume of the hydrogen ion (m^3 mol^{-1})
V_-	molar volume of the hydrogen sulfate ion (m^3 mol^{-1})
$V_{p,i}$	molar volume of product (m^3 $kmol^{-1}$)
$V_{r,i}$	molar volume of reactant (m^3 $kmol^{-1}$)
x	distance (m)
X	degree of discharge
z	dimensionless distance

Greek letters

a,	cathodic transfer coefficient
ϵ	porosity
ϵ_g	fraction of electrode cross-sectional area
ϵ_m	porosity of the active material
η	overvoltage (V)
η'	dimensionless overvoltage
κ	conductivity (Ω^{-1} m^{-1})
A	ratio between effective and free transport parameters
ρ	density (kg m^{-3})
ϕ	potential (V)
τ	dimensionless time

Subscript

0	initial value
e	electrode
eff	effective value
n	negative electrode
p	positive electrode
s	separator
W	water

Superscript

0	initial value

Acknowledgements

This work was financially supported by the Swedish National Board for Industrial and Technical Development. We thank Tudor AB in Nol, Sweden, for their supply of electrodes to this experimental program.

The financial support from the Royal Swedish Academy and Natural Sciences and Engineering Research Council of Canada for the participation of Mr Artjom Sokirko in the present work is gratefully acknowledged.

Appendix

Stability and conservative properties of the numerical solution

The algorithm developed by Newman [19] provides a stable solution for a linear system, independently of the variation of the time step. For non-linear systems stability can be achieved only for a finite time step, which, as a rule, can only be determined after numerical experiments. Nonetheless, not even a very small time step can guarantee the stability of numerical calculations. There are several causes for an instability of the numerical algorithm, e.g.:

(i) Instability due to the linearization of non-linear coefficients and terms. In the case that we solve non-linear equations, we have to decide up to what extent we are going to approximate the non-linear terms. For example, in the calculation of a diffusion coefficient

on the next time level according to Eq. (24), we have to substitute some value for the concentration in the expression for D(C). It is evident to use the value of the concentration from the previous time step. Otherwise, a system of linear algebraic equations cannot be obtained. This gives a satisfactory result when coefficients are changing slowly with time and distance, otherwise an instability will appear. For example, it occurs when we have a significant concentration gradient.

(ii) Instability due to *initial conditions.* In our case there are no problems with initial values of porosity and concentration profiles. On the contrary, the initial potential distribution is not known and must be found from the solution of the equation for the potential before the real calculation can start. In the opposite case, when an initial potential distribution is not well defined, the values of the overpotential from the previous time step, involved into the non-linear terms (even after linearization), can lead to instability.

(iii) Instability due to the *conditions at the interface.* This may be illustrated by the simplest example of Eq. (11a). If the lengths of the space steps inside the separator and the electrode are equal to each other and the number of interface points is n, then this condition can be approximated as $D^{p}_{eff}(C_n - C_{n-,}) = D^{s}_{eff}(C_{n+1} - C,)$. From that expression we can combine a 'production' term $\partial^2 C/\partial z^2 = (C_{n+,} - 2C_n + C_{n-1})/\Delta h^2$ which, roughly speaking, must correspond to the consumption of matter in the interface region. However, it does not. When $D^{p}_{eff} = D^{s}_{eff}$, we have $\partial^2 C/\partial z^2 = 0$, while the production must vanish under completely different conditions – the absence of an available active surface in the boundary region of the electrode. Therefore, there is an inaccuracy, generally inversely proportional to the number of grid points, but increasing significantly in typical situations when a discharge mostly takes place in the electrode in this, the most accessible, part of electrode. Such an inaccuracy of 10 or even 20% can cause a loss of stability.

We have to note that such an effect is not directly correlated with the accuracy of the approximation of the boundary conditions. Moreover, as it was first noted by Arakawa [20], three-point approximations for boundary conditions, as a rule, have much worse stability than the two-point ones. This is probably why the algorithm for solution with five-diagonal matrix described in Ref. [17], turned out not to work for our problem.

In conclusion, 'interface conditions' must be avoided whenever it is possible.

(iv) Instability due to *boundary conditions.* The stability of a numerical solution also depends upon the ratio of the numbers of boundary conditions for functions and derivatives. The boundary conditions for functions improve stability, while boundary conditions for derivatives make the stability worse. It is connected with some fundamental properties of the original Thomson algorithm and that cannot be analysed here in detail. Note, however, that the direction in which the differential equation is solved is also important, although from a mathematical point of view these problems are equivalent. If we start from a definite value of the function on one edge and meet the conditions for derivative on the other end, we will have a better result than in the opposite case, when we start from the derivative.

In our problem there are no boundary conditions for porosity and all boundary conditions for concentration and potential are conditions for their derivatives, which leads to a formal instability of the linearized homogeneous system. This phenomenon can be easily understood. If a differential equation does not include the function itself but only its first and second derivatives, a function, different by a constant, will be a solution of this equation and boundary conditions. Moreover, two boundary conditions for derivatives can contradict each other. Therefore, we have to admit, that a straightforward application of Newman's technique [18] to the linearized system sometimes can involve serious mathematical and numerical difficulties. Note that, strictly speaking, our speculation is valid only for linearized elliptic systems. Of course, the full system of parabolic equations (Eqs. (1) to (8)) with initial conditions (Eq. (9)) and boundary conditions (Eqs. (10) to (12)) are self-consistent from a mathematical point of view. The values of function C and X cannot be set arbitrarily, because they depend on the initial conditions as well.

The conservativity of a numerical scheme is a measure of how long it is able to describe the model system with necessary accuracy. In some sense conservativity is a result of a good precision and stability. At the same time conservativity is a wider concept, because it requires that some additional parameters keep their values. For example, on one hand, in our case of galvanostatic discharge, the total amounts of H_2SO_4, Pb and PbO_2 must change linearly with time, because the electrochemical reactions are subject to Faraday's law. On the other hand, these additional conditions do not follow directly from discretised equations and boundary conditions.

There are two main reasons why the system can loose conservativity:

(i) *Numerical.* All the above-mentioned reasons for non-stability can interfere with conservativity as well. We also have to note that there is no general algorithm for the construction of a conservative numerical scheme for non-linear differential equations, as those appearing in the used model. Actually, the only way to improve conservativity is to perform the calculations at each time level with sufficient precision. Our experience shows that although there are no theoretical restrictions

on the choice of a grid step inside each region, a uniform space step for all regions gives a much more conservative numerical scheme. Therefore, in the computer experiments presented in this paper, we always use a uniform grid, choosing the number of grid points in such a way that interface points placed halfway between two grid points are as accurate as possible.

(ii) Model. Some model approximations also can lead to non-conservative solutions. For example, it is generally accepted that the transference number depends only on concentration and does not depend on current density. Of course, this dependence is rather slow, but integration of it with time, at a high gradient of current density, can give us a significant departure for conservativity.

Taking into account all the above-mentioned factors, we have constructed our own numerical algorithm. This algorithm, although it is not as transparent as those of Newman [19] and White [17], gives us the possibility of a stable, accurate and fast modelling for any value of the input parameters up to a high degree of discharge. The minimal dimensionless concentration inside the electrode can be as small as 0.005.

References

[1] K. Micka and I. Roušar, ***Electrochim. Acta, 21*** (1976) 599.

[2] W.H. Tiedemann and J. Newman, in S. Gross (ed.), ***Battery Design and Optimization,*** The Electrochemical Society Softbound Proceedings Series, Princeton, NJ, USA, 1979, p. 23.

[3] W.G. Sunu, in R.E. White (ed.), ***Electrochemical Cell Design,*** Plenum, New York, 1984, p. 357.

[4] H. Gu, T.V. Nguyen and R.E. White, ***J. Electrochem. Soc., 134*** (1987) 2953.

[5] T.V. Nguyen, R.E. White and H. Gu, ***J. Electrochem. Soc., 137*** (1990) 2998.

[6] T.V. Nguyen and R.E. White, ***Electrochim. Acta, 38*** (1993) 935.

[7] D.M. Bernardi, H. Gu and A.Y. Schoene, ***J. Electrochem. Soc., 140*** (1993) 2250.

[8] M. Maja, G. Morello and P. Spinelli, ***J. Power Sources, 40*** (1992) 81.

[9] J. Landfors, ***J. Power Sources,*** accepted for publication.

[10] J. Newman and W. Tiedemann, ***AIChE J.,*** 21 (1975) ***25.***

[11] P. Ekdunge and D. Simonsson, ***J. Appl. Electrochem., 19*** (1989) 136.

[12] K. Micka and I. Rousar, ***Electrochim. Acta,*** 18 (1973) 629.

[13] J. Vittonato, ***Thesis,*** Department of Applied Electrochemistry, The Royal Institute of Technology, March 1991.

[14] D. Simonsson, ***J. Appl. Electrochem., 3*** (1973) 261.

[15] J. Landfors and D. Simonsson, ***J. Electrochem. Soc.,*** 139 (1992) 2768.

[16] R.E. White, ***Ind. Eng. Chem. Fundam., 17*** (1978) 267.

[17] D. Fan and R.E. White, ***J. Electrochem. Soc., 138*** (1991) 1688.

[18] K.W. Choi and N.P. Yao, ***J. Electrochem. Soc., 125*** (1978) 1011.

[19] J.S. Newman, ***Electrochemical Systems,*** Prentice-Hall, Englewood Cliffs, NJ, 1991, pp. 539-555.

[20] A. Arakawa, ***J. Comput. Phys., 1*** (1966) 119.